

Angular distribution of Ly α resonant photons emergent from optically thick medium

Yang Yang¹, Ishani Roy², Chi-Wang Shu¹ and Li-Zhi Fang³

ABSTRACT

We investigate the angular distribution of Ly α photons transferring in or emergent from an optically thick medium. Since the evolutions of specific intensity I in the frequency space and the angular space are coupled from each other, we first develop the WENO numerical solver in order to find the time-dependent solutions of the integro-differential equation of I in the space of frequency and angular simultaneously. We show first that the solutions with the Eddington approximation, which assume I to be linearly dependent on the angular variable μ , yield similar frequency profiles of the photon flux as that without the Eddington approximation. However, the solutions of the μ distribution evolution are significantly different from that given by Eddington approximation. First, the angular distribution of I are found to be substantially dependent on the frequency of photons. For photons with the resonant frequency ν_0 , I contains only a linear term of μ . For photons with frequency at the double peaks of the flux, the μ -distribution is highly anisotropic, in which most photons are in the direction of radial forward. Moreover, either at ν_0 or at the double peaks, the μ distributions actually are independent of the initial μ distribution of photons of the source. This is because the photons with frequency either of ν_0 or of the double peaks have undergone the process of forgetting their initial conditions due to the resonant scattering. We also show that the optically thick medium is a collimator of photons at the double peaks. Photons from the double peaks form a forward beam with very small spread angle.

Subject headings: cosmology: theory - intergalactic medium - radiation transfer - scattering

¹Division of Applied Mathematics, Brown University, Providence, RI 02912, USA

²Imaging Sciences & Biomedical Engineering Division, St Thomas Hospital, Kings College London, SE1 7EH, UK

³Department of Physics, University of Arizona, Tucson, AZ 85721, USA

Report Documentation Page

Form Approved
OMB No. 0704-0188

Public reporting burden for the collection of information is estimated to average 1 hour per response, including the time for reviewing instructions, searching existing data sources, gathering and maintaining the data needed, and completing and reviewing the collection of information. Send comments regarding this burden estimate or any other aspect of this collection of information, including suggestions for reducing this burden, to Washington Headquarters Services, Directorate for Information Operations and Reports, 1215 Jefferson Davis Highway, Suite 1204, Arlington VA 22202-4302. Respondents should be aware that notwithstanding any other provision of law, no person shall be subject to a penalty for failing to comply with a collection of information if it does not display a currently valid OMB control number.

1. REPORT DATE 26 FEB 2012	2. REPORT TYPE	3. DATES COVERED 00-00-2012 to 00-00-2012			
4. TITLE AND SUBTITLE Angular distribution of Lyα; resonant photons emergent from optically thick medium		5a. CONTRACT NUMBER			
		5b. GRANT NUMBER			
		5c. PROGRAM ELEMENT NUMBER			
6. AUTHOR(S)		5d. PROJECT NUMBER			
		5e. TASK NUMBER			
		5f. WORK UNIT NUMBER			
7. PERFORMING ORGANIZATION NAME(S) AND ADDRESS(ES) Brown University, Division of Applied Mathematics, Providence, RI, 02912		8. PERFORMING ORGANIZATION REPORT NUMBER TR-2012-04			
9. SPONSORING/MONITORING AGENCY NAME(S) AND ADDRESS(ES)		10. SPONSOR/MONITOR'S ACRONYM(S)			
		11. SPONSOR/MONITOR'S REPORT NUMBER(S)			
12. DISTRIBUTION/AVAILABILITY STATEMENT Approved for public release; distribution unlimited					
13. SUPPLEMENTARY NOTES					
14. ABSTRACT <p>We investigate the angular distribution of Lyα; photons transferring in or emergent from an optically thick medium. Since the evolutions of specific intensity I in the frequency space and the angular space are coupled from each other, we first develop the WENO numerical solver in order to find the time-dependent solutions of the integro-differential equation of I in the space of frequency and angular simultaneously. We show first that the solutions with the Eddington approximation, which assume I to be linearly dependent on the angular variable μ, yield similar frequency profiles of the photon flux as that without the Eddington approximation. However, the solutions of the μ distribution evolution are significantly different from that given by Eddington approximation. First, the angular distribution of I are found to be substantially dependent on the frequency of photons. For photons with the resonant frequency ω_0, I contains only a linear term of μ. For photons with frequency at the double peaks of the flux, the μ-distribution is highly anisotropic, in which most photons are in the direction of radial forward. Moreover, either at ω_0 or at the double peaks, the μ distributions actually are independent of the initial μ distribution of photons of the source. This is because the photons with frequency either of ω_0 or of the double peaks have undergone the process of forgetting their initial conditions due to the resonant scattering. We also show that the optically thick medium is a collimator of photons at the double peaks. Photons from the double peaks form a forward beam with very small spread angle.</p>					
15. SUBJECT TERMS					
16. SECURITY CLASSIFICATION OF:			17. LIMITATION OF ABSTRACT Same as Report (SAR)	18. NUMBER OF PAGES 23	19a. NAME OF RESPONSIBLE PERSON
a. REPORT unclassified	b. ABSTRACT unclassified	c. THIS PAGE unclassified			

1. Introduction

The transfer of Ly α photons in an optically thick medium consisting of neutral hydrogen atoms is fundamentally important, as Ly α photon is an effective tool to study the physics of luminous objects at various epochs of the universe. It includes Ly α emitters, Ly α blob, damped Ly α system, Ly α forest, fluorescent Ly α emission, star-forming galaxies, quasars at high redshifts as well as optical afterglow of gamma ray bursts (Haiman et al. 2000; Fardal et al. 2001; Dijkstra & Loeb 2009; Latif et al. 2011). Ly α photons emergent from an optically thick halo surrounding a source of the Ly α photon would be useful to constrain the mass density, velocity, temperature and the fraction of neutral hydrogen of the optically thick halo.

The radiative transfer of resonant photons has been extensively studied analytically and numerically for more than half a century. An early effort (Adams et al. 1971) only focused on the numerical approximation of the redistribution function of resonant scattering, and no solution of the integro-differential equation of the radiative transfer has been found. The first analytical solution of the integro-differential equation is given by Field (1958) for the case of both medium and source to be uniformly distributed in the whole space. Analytical solutions of the frequency profile of photons emergent from optically thick halo are also found based on the Fokker-Planck (P-F) approximation of the integro-differential equation (Harrington 1973; Neufeld 1990; Dijkstra et al. 2006). Monte Carlo (MC) simulations are also popular in solving the transfer of resonant photons (e.g. Loeb & Rybicki 1999; Zheng & Miralda-Escude 2002; Tasitsiomi 2006; Verhamme et al. 2006; Laursen & Sommer-Larsen 2007; Pierleoni et al. 2009; Xu & Wu 2010; Xu et al. 2011).

Nevertheless, many important topics cannot be seen with the above-mentioned solutions. Besides the Field's analytical solution, all others are time-independent, and therefore, they cannot even be used to describe the formation and evolution of the Wouthuysen-Field (W-F) local thermalization of the Ly α photon frequency distribution (Wouthuysen 1952; Field 1958, 1959). The rich features of the Ly α photon transfer referring to the W-F local thermalization are fully missed. The P-F equation is based on the Eddington approximation, which assumes that the radiation intensity is a linear function of angular (direction) variable. The solutions of the P-F equation do not provide the information of the evolution of the angular distribution of Ly α photons.

Recently, a solver of the radiative transfer of resonant photon has been developed based on the weighted essentially non-oscillatory scheme (WENO), which is a good numerical solver of the hydrodynamic equations and the kinetic equations (Jiang & Shu 1996). With the WENO solver, many interesting features of Ly α resonant photon transfer have been revealed. It shows that the double peaked frequency profile of the Ly α photon emergent from an optically thick medium generally does not follow the time-independent solutions of the P-F equation (Fang 2009; Roy et al. 2009a, 2009b, 2009c, 2010). The solver has also been used to calculate time-dependent features: 1) the timescale of the formation of the W-F effect; 2) the light-curve of a flash source

surrounded by optically thick halo; 3) the dependence of the Ly α photon escape coefficient on the redshifts of sources; 4) the effects of dust on the double-peak profile of the emergent Ly α photons (Roy et al. 2009a, 2009b, 2009c, 2010; Yang et al. 2011; Xu et al. 2011). These features have not been seen with previous methods.

This paper will study the angular distribution of Ly α photon transferring in an optically thick medium. As mentioned above, the evolution of the angular distribution is completely ignored in all the methods based on the Eddington approximation. The evolution of angular distribution actually is significant. In a thermalized or statistical equilibrium state, the angular distribution of photons should be isotropic, regardless of the initial angular distribution. Therefore, one can expect that the angular distribution of Ly α photons with resonant frequency ν_0 should be isotropic. On the other hand, the angular distribution of photons with frequency different from ν_0 might be anisotropic, as those photons are not involved in the evolution of thermalization or statistical equilibrium. Consequently, the angular distributions of Ly α resonant photons from optically thick medium should be frequency-dependent. It definitely cannot be described by the Eddington approximation. The evolution of the angular distribution of resonant photons is not trivial. We still use the WENO solver. In this case, we should first develop the WENO solver to be able to simultaneously solve the photon transfer in both frequency- and angular spaces.

The paper is organized as follows. Section 2 presents the basic features of Ly α photon transfer given by the WENO solver. In section 3, the precision of the Eddington approximation will be studied via a comparison between solutions with and without the Eddington approximation. Section 4 presents the results of the evolution of the angular distribution, especially, on the frequency-dependence, source-dependence and position-dependence of the Ly α photon angular distribution. The discussion and conclusion are given in Section 5. Mathematical details of the WENO algorithm on the radiative transfer equation are given in the Appendix.

2. WENO solver of transfer equations of resonant photons

The WENO solver, some details of which being given in the Appendix, is to solve the following radiative transfer equation of Ly α resonant photon in a spherical symmetric medium containing neutral HI.

$$\frac{\partial I}{\partial \eta} + \mu \frac{\partial I}{\partial r} + \frac{(1 - \mu^2)}{r} \frac{\partial I}{\partial \mu} - \gamma \frac{\partial I}{\partial x} = -\phi(x; a)I + \int \mathcal{R}(x, x'; a)I(\eta, r, x', \mu') dx' d\mu' / 2 + S, \quad (1)$$

where $I(t, r_p, x, \mu)$ is the specific intensity, which is a function of time t , radial coordinate r_p , frequency x and $\mu = \cos \theta$, the direction angle with respect to the radial vector \mathbf{r} . $S(\eta, r_p, x, \mu)$ is

the source of photons.

In eq.(1), we use the dimensionless time η defined as $\eta = cn_{\text{HI}}\sigma_0 t$ and the dimensionless radial coordinate r defined as $r = n_{\text{HI}}\sigma_0 r_p$, where n_{HI} is the number density of HI, and $\sigma_0/\pi^{1/2}$ is the cross section of HI resonant scattering of Ly α photons at resonant frequency $\nu_0 = 2.46 \times 10^{15} \text{ s}^{-1}$. That is, η and r are, respectively, in the units of mean free flight-time and mean free path of photon ν_0 with respect to the resonant scattering without dust scattering and absorption. Without resonant scattering, a signal propagates in the radial direction with the speed of light, the orbit of the signal is then $r = \eta + \text{const}$.

$\phi(x, a)$ is the normalized Voigt profile (Hummer 1965) given as

$$\phi(x, a) = \frac{a}{\pi^{3/2}} \int_{-\infty}^{\infty} dy \frac{e^{-y^2}}{(x-y)^2 + a^2}. \quad (2)$$

As usual, the photon frequency ν in eq.(2) is described by the dimensionless frequency $x \equiv (\nu - \nu_0)/\Delta\nu_D$, and $\Delta\nu_D = \nu_0(\nu_T/c) = 1.06 \times 10^{11}(T/10^4)^{1/2} \text{ Hz}$ is the Doppler broadening by the thermal motion $\nu_T = \sqrt{2k_B T/m_{\text{HI}}}$, T being the gas temperature of the halo. The parameter a in eq.(2) is the ratio of the natural to the Doppler broadening. For the Ly α line, $a = 4.7 \times 10^{-4}(T/10^4)^{-1/2}$. The optical depth of Ly α photons with respect to HI resonant scattering is $d\tau_s(x) = n_{\text{HI}}\sigma(x)dr_p$, where $\sigma(x) = \sigma_0\phi(x, a)$ is the cross section of scattering at ν , and therefore, the dimensionless size of the halo R is equal to the optical depth $\tau_0 = n_{\text{HI}}\sigma_0 R$.

The re-distribution function $\mathcal{R}(x, x'; a)$ of eq.(2) gives the probability of a photon absorbed at the frequency x' , and re-emitted at the frequency x . It depends on the details of the scattering (Henyey & Greestein 1941; Hummer 1962; Hummer 1969). If we consider coherent scattering without recoil, the re-distribution function with the Voigt profile is

$$\mathcal{R}(x, x'; a) = \frac{1}{\pi^{3/2}} \int_{|x-x'|/2}^{\infty} e^{-u^2} \left[\tan^{-1} \left(\frac{x_{\min} + u}{a} \right) - \tan^{-1} \left(\frac{x_{\max} - u}{a} \right) \right] du, \quad (3)$$

where $x_{\min} = \min(x, x')$ and $x_{\max} = \max(x, x')$. In the case of $a = 0$, i.e. considering only the Doppler broadening, the re-distribution function is

$$\mathcal{R}(x, x') = \frac{1}{2} \text{erfc}[\max(|x|, |x'|)]. \quad (4)$$

The re-distribution function of equation (4) is normalized as $\int_{-\infty}^{\infty} \mathcal{R}(x, x') dx' = \phi(x, 0) = \pi^{-1/2} e^{-x^2}$. With this normalization, the total number of photons is conserved in the evolution described by equation (3). That is, the destruction processes of Ly α photons, such as the two-photon process (Spitzer & Greenstein 1951; Osterbrock 1962), are ignored in equation (3). The recoil of atoms is not considered in equation (3) or (4). The dust absorption is also ignored.

For Dipole scattering, eq.(4) should be replaced by (Hummer 1962)

$$\mathcal{R}(x, x') = \frac{3}{8} \left\{ \frac{1}{2} \operatorname{erfc}[\max(|x|, |x'|)] [3 + 2(x^2 + x'^2) + 4x^2 x'^2] - \frac{\max(|x|, |x'|)}{\sqrt{\pi}} \exp[-\max(|x|, |x'|)] [2|\min(|x|, |x'|)|^2 + 1] \right\}, \quad (5)$$

which is still μ -independent.

In eq. (1), the term with the parameter γ is due to the expansion of the universe. If n_{HI} is equal to the mean of the number density of cosmic hydrogen, we have $\gamma = \tau_{\text{GP}}^{-1}$, and τ_{GP} is the Gunn-Peterson optical depth. Since the Gunn-Peterson optical depth is of the order of 10^6 at high redshift (e.g. Roy et al. 2009c), the parameter γ is of the order of $10^{-5} - 10^{-6}$. Therefore, if the optical depth of halos is equal to or less than 10^6 , the term with γ of eq.(1) can be ignored.

2.1. Test with Field's analytical solution

The WENO solver used in this paper is different from the previous version (Roy et al. 2009a, 2009b, 2009c). In the previous version, the evolution of I in the μ -space is eliminated by the Eddington approximation, while the current solver treats the evolution of I in the μ -space governed by eq.(1).

We first test the WENO solver with analytical solutions. Assuming that the specific intensity and source S are homogeneous in the r and μ space, i.e. $I(\eta, r, x, \mu)$ is independent of variables r and μ . Eq.(1) becomes

$$\frac{\partial J}{\partial \eta} - \gamma \frac{\partial J}{\partial x} = -\phi(x)I + \int R(x, x')J(\eta, x')dx' + S, \quad (6)$$

where

$$J(\eta, x) = \frac{1}{2} \int I(\eta, r, x, \mu)d\mu. \quad (7)$$

Take $\gamma = 0$, Doppler parameter $a = 0$, the source $S = \phi(x) = \pi^{-1/2}e^{-x^2}$, and the initial radiative field $I(x, \eta = 0) = 0$. The time-dependent solution of eq.(6) is (Field 1958, Rybicki & Dell'Antonio 1994)

$$J(x, \eta) = \pi^{-1/2} [1 - \exp(-\eta e^{-x^2})] + \int_x^\infty e^{w^2} [1 - (1 + \eta e^{-w^2}) \exp(-\eta e^{-w^2})] \operatorname{erf}(w) dw. \quad (8)$$

Our solver is to directly find the solution I from eq.(1). One can then give J via eq.(7). It is interesting to see whether the solution eq.(8) can be reproduced, if we also assume that the source

S in eq.(1) is spatially homogeneous, but μ -dependent, i.e. $S = \Theta(\mu)\phi(x) = \Theta(\mu)\pi^{-1/2}e^{-x^2}$ where $\Theta(\mu)$ describes the angular distribution of photons from the source. We consider the source as follows,

$$S = \begin{cases} 2(n+1)\mu^n\pi^{-1/2}e^{-x^2}, & 0 < \mu \leq 1, \\ 0, & -1 \leq \mu \leq 0, \end{cases} \quad (9)$$

where n is taken to be a positive integer. Obviously, the source is isotropic when $n = 0$, while it is anisotropic if $n \neq 0$. The larger the n , the stronger the emission in the direction $\mu = 1$. The factor $2(n+1)$ is for normalization: $\frac{1}{2} \int_0^1 2(n+1)\mu^n d\mu = 1$.

The numerical results with sources $n = 0, 4$ and 6 are shown in Fig. 1. It is expected that the

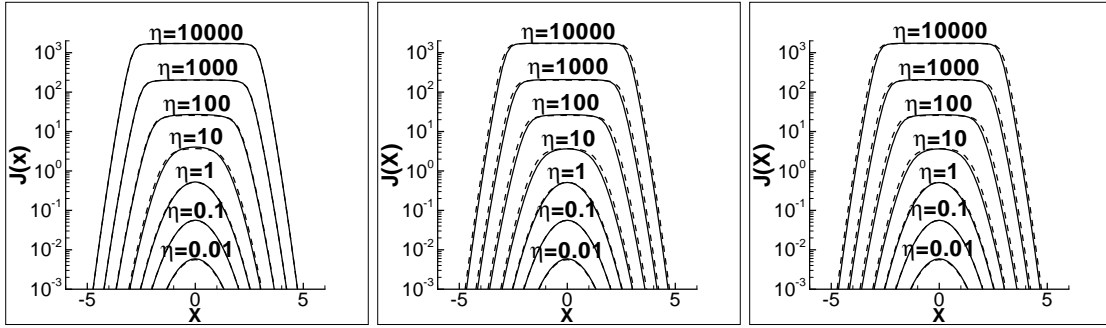


Fig. 1.— The WENO numerical solutions (solid lines) of eq.(1) assuming the sources S is a) $S = \pi^{-1/2}e^{-x^2}$ for all μ (left); b) $S = 10\mu^4\pi^{-1/2}e^{-x^2}$ (middle); and c) $S = 14\mu^6\pi^{-1/2}e^{-x^2}$ (right) for $\mu > 0$ and $S=0$ for $\mu < 0$. The Field's analytical solution is shown with dot lines.

numerical solution of $n = 0$ (the left panel of Fig.1) should follow the analytical solution eq.(8) well, as the isotropic source is the same as that used to find the analytical solution.

It is interesting to see that the WENO solutions of $n = 4$ (middle panel) and $n = 6$ (right panel) also follow the analytical solution eq.(8) well. It seems to indicate that the evolution of the frequency space is independent of that of the μ -space.

2.2. Time scale of the statistical equilibrium of the angular distribution

A remarkable feature of the solutions of Fig. 1 is to show a flat plateau in the range $|x| < 2$ at time $\eta > 100$. The flat plateau is caused by the Wouthuysen-Field local thermalization of frequency distribution of resonant photon (Wouthuysen 1952; Field 1958, 1959). The flat plateau actually is the Boltzmann statistical equilibrium distribution around $x = 0$ when the atomic mass is infinite. If the mass is finite, i.e. considering the recoil in the re-distribution functions (3) or (4), the flat

plateau will become e^{-2bx} , where $b = hv_0/mv_Tc$. This is the local Boltzmann distribution required by the Wouthuysen-Field effect (Roy et al. 2009b). The resonant scattering between photons and HI atoms leads to the Boltzmann distribution of the photon frequency distribution around $x = 0$ with the temperature equal to that of HI atoms.

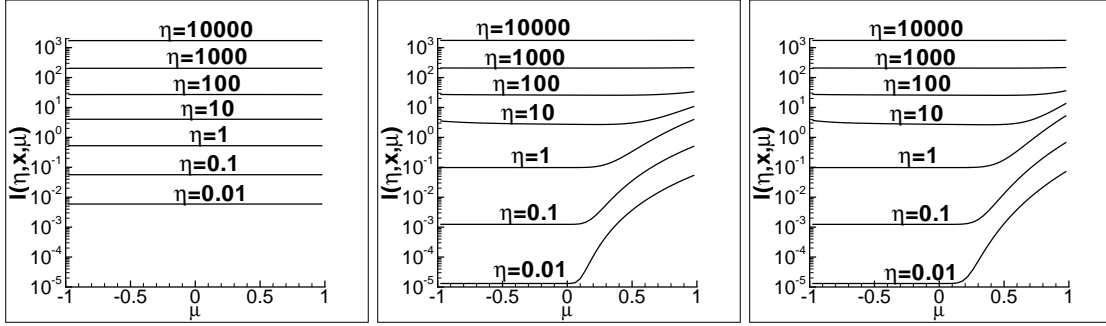


Fig. 2.— The WENO numerical solutions of angular distributions from eq.(1) at $x = 0$, assuming the sources S are a) $S = \pi^{-1/2}e^{-x^2}$ for all μ (left) and b) $S = 10\mu^4\pi^{-1/2}e^{-x^2}$ (middle); and c) $S = 14\mu^6\pi^{-1/2}e^{-x^2}$ (right) for $\mu > 0$ and $S=0$ for $\mu < 0$.

When resonant photons undergo the local thermalization in the frequency space, the angular distribution should undergo the evolution of approaching statistical equilibrium. The anisotropic μ -distributions have to evolve to isotropic (statistical equilibrium). We calculate all the μ -distributions at the time η corresponding to the three panels of Fig. 1. The result is plotted in Fig. 2. The μ -distribution of left panel is always isotropic. This is expected as the source is isotropic, which is already in the state of statistical equilibrium.

The middle and right panels of Fig. 2 show the evolution of an anisotropic μ -distribution eq.(9) to isotropic. The time scale of approaching isotropic distribution seems to be independent of the anisotropy of sources. It is always equal to about $\eta \sim 100$ for both $n = 4$ and $n = 6$, i.e. the μ -distribution will become isotropic after 100 times of resonant scattering. This time scale is about the same as that of the W-F thermalization (Fig. 1). Therefore, the thermalization in the frequency space and the isotropic distribution in the μ -space are realized at about the same time.

3. Precision of the Eddington approximation

3.1. Equations of the Eddington approximation

We now consider the transfer of Ly α photons in a spherical halo with an optical source at its center. The halo is assumed to consist of uniformly distributed HI gas with number density n_{HI} . The μ -dependence of the specific intensity I can generally be expressed by a Legendre expansion $I(\eta, r, x, \mu) = \sum_l I_l(\eta, r, x) P_l(\mu)$. The Eddington approximation is to take only the first two terms of the Legendre expansion, and drop all terms of $l \geq 2$ (e.g. Rybicki & Lightman, 1979). That is

$$I(\eta, r, x, \mu) \simeq J(\eta, r, x) + 3\mu F(\eta, r, x), \quad (10)$$

where

$$J(\eta, r, x) = \frac{1}{2} \int_{-1}^{+1} I(\eta, r, x, \mu) d\mu, \quad F(\eta, r, x) = \frac{1}{2} \int_{-1}^{+1} \mu I(\eta, r, x, \mu) d\mu. \quad (11)$$

They are, respectively, the angularly averaged specific intensity and flux.

Defining $j = r^2 J$ and $f = r^2 F$, eq.(1) yields the equations of j and f as

$$\frac{\partial j}{\partial \eta} + \frac{\partial f}{\partial r} = -\phi(x; a)j + \int \mathcal{R}(x, x'; a) j dx' + \gamma \frac{\partial j}{\partial x} + r^2 S, \quad (12)$$

$$\frac{\partial f}{\partial \eta} + \frac{1}{3} \frac{\partial j}{\partial r} - \frac{2}{3} \frac{j}{r} = -\phi(x; a)f + \gamma \frac{\partial f}{\partial x}. \quad (13)$$

The mean specific intensity $j(\eta, r, x)$ describes the x photons trapped in the position r at time η by the resonant scattering, while the flux $f(\eta, r, x)$ describes the photons in transit. One can test the precision of the Eddington approximation by a comparison of the solution of eq.(1) without Legendre expansion with that of the Eddington approximation.

3.2. Profiles of j and f

For spherical halo with a central source, the term S of eq.(1) can be replaced by a boundary condition of $I(\eta, r, x, \mu)$ at $r = 0$. If the angular distribution of photon is independent of photon's frequency, we have generally

$$r^2 I(\eta, r, x, \mu)|_{r=0} = S_0 T(\eta) \Theta(\mu) \phi(x). \quad (14)$$

where the functions $T(\eta)$, $\Theta(\mu)$, and $\phi(x)$ describe, respectively, the time-dependence, angular- and frequency-distributions of photons of the source. The factor S_0 gives the intensity of the source.

In this case, the source of eq.(12) can be replaced by a boundary condition at $r = 0$ as

$$j(\eta, 0, x) = 0, \quad f(\eta, 0, x) = S_0 T(\eta) \phi(x) \frac{1}{2} \int \mu \Theta(\mu) d\mu. \quad (15)$$

On the outside of the halo, $r > R$, no photons propagate in the direction $\mu < 0$. The boundary condition at $r = R$ of eq.(1) should be

$$I(\eta, R, x, \mu) = 0, \quad \mu < 0. \quad (16)$$

For eq.(12), we have $\int_0^{-1} \mu I(\eta, R, x, \mu) d\mu = 0$ (Unno 1955), the boundary condition is then

$$j(\eta, R, x) = 2f(\eta, R, x). \quad (17)$$

If the source starts to emit photon at $t = 0$, the initial condition should be

$$I(0, r, x, \mu) = 0, \quad (18)$$

for eq.(1), and

$$j(0, r, x) = f(0, r, x) = 0, \quad (19)$$

for eq.(12).

We solve eq.(1) by taking the boundary condition at $r = 0$ to be

$$r^2 I(\eta, r, x, \mu)|_{r \rightarrow 0} = \begin{cases} 6\mu\pi^{-1/2}e^{-x^2}, & \mu > 0, \\ 0, & \mu < 0. \end{cases} \quad (20)$$

With eq.(20) one can find I from eq.(1), and then find j and f via eqs.(11). The results are given in the right panels of Fig. 3, which shows the well-known double peaks at $|x| \sim 2$.

With eq.(20), the corresponded boundary condition of eq.(15) is

$$j(\eta, r = 0, x) = 0, \quad f(\eta, r = 0, x) = \pi^{-1/2}e^{-x^2}. \quad (21)$$

The profiles of j and f given by the solutions of eqs.(11) and (12) and condition eq.(21) are shown in the left panels of Fig.3. The profiles on the left and right panels in Fig.3 are about the same, indicating that the Eddington approximation is a good one for this case.

To replace the factor 6μ of eq.(20) with $\Theta(\mu) = 16\mu^6$, we re-do the solution of j and f with eq.(1). The results are given in Fig.4, which still shows the same shape of the profiles as that of the left panels of Fig.3. That is, the profiles of j and f are not affected by the angular distribution of photons from the source. It is probably because the μ -distribution quickly evolves into the statistical equilibrium state, the initial anisotropy of the μ distribution is forgotten.

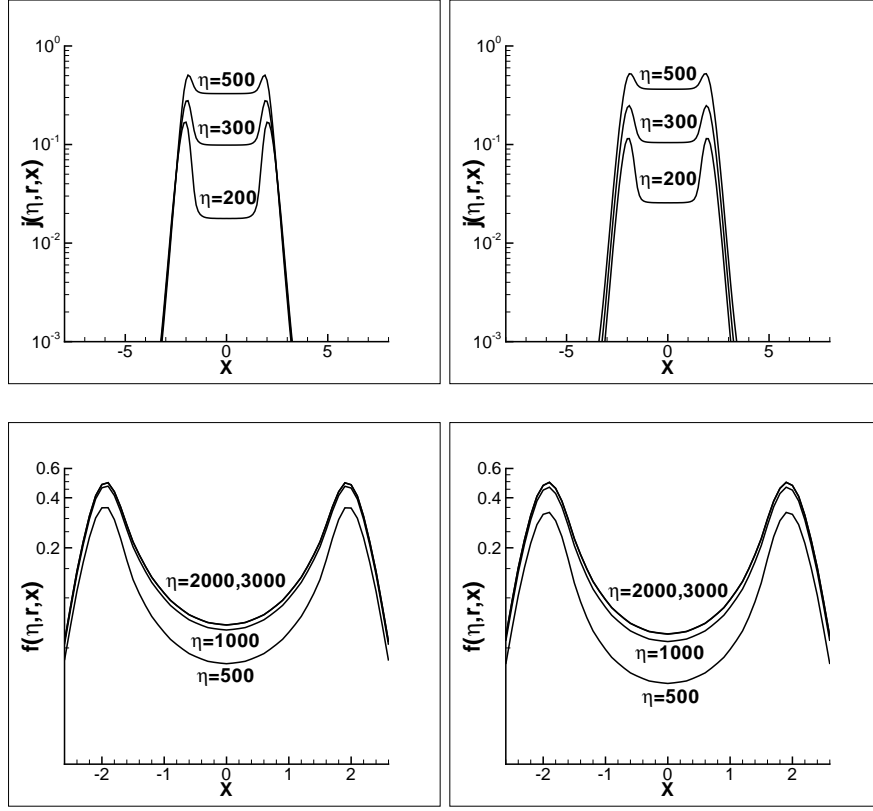


Fig. 3.— A comparison of the solutions j (top) and f (bottom) with the Eddington approximation (left) and the solutions of j and f without the Eddington approximation (right). Relevant parameters are $R = 10^2$, and $a = 10^{-3}$.

Nevertheless, Figs. 3 and 4 do show small differences between the solutions with and without the Eddington approximation, even though both solutions are given by the same source. The difference comes from the contribution of the terms of $l > 2$ in the Legendre expansion. The difference between the profiles with and without the Eddington approximation becomes smaller when the time η is larger. It is because larger η corresponds to larger optical depth. The Eddington approximation generally is good for optically thick medium.

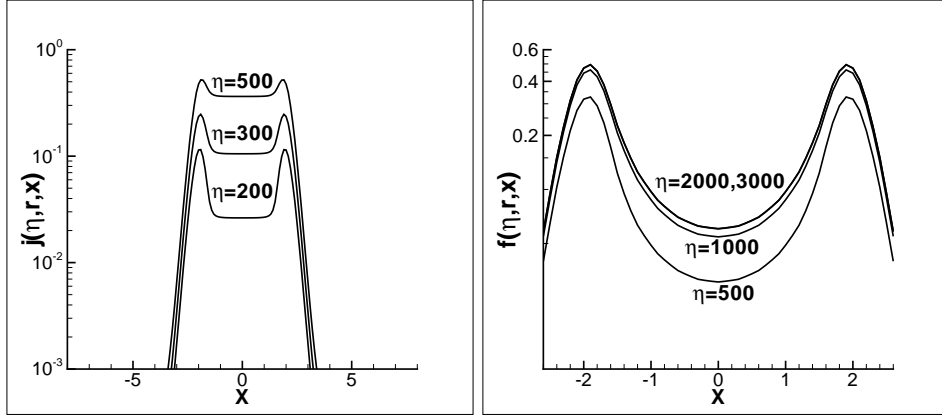


Fig. 4.— The same as the right panels of Fig. 3, but the μ -distribution 6μ of the source eq.(20) is replaced by $16\mu^6$.

4. Angular distributions

4.1. Frequency dependence

Although the Eddington approximation is acceptable to calculate the profile of Ly α photons in the frequency space, it would fail in the μ -space. The result of Fig. 2 shows that the μ -distribution is isotropic at frequency ν_0 . On the other hand, the μ -distribution will no longer be isotropic at frequency $|x| \geq 2$, because photons of $|x| \geq 2$ have not undergone enough number of scattering. Consequently, the angular distribution of photons emergent from optically thick halo should be frequency(energy)-dependent.

We calculate the μ -distribution of photons from halo with $R = 500$ with the central source given by eq.(20), i.e. photons from the source can be described by the Eddington approximation eq.(10). The result is shown in Fig.5. The μ distributions at frequencies $x = 0$ (top left panel of Fig. 5) and 0.8 (top right) basically are straight lines in the whole range $-1 \leq \mu \leq 1$. That is, I can be described by the Eddington approximation eq.(10).

At $x = 1.6$ (bottom left panel of Fig. 5), the μ -distribution starts to deviate from a straight line, i.e. deviating from an Eddington approximation. At $x = 2.4$ (bottom right), the μ -distribution shows a very sharp spike at $\mu = 1$. That is, the angular distribution of photons with frequency at the two peaks (Fig. 3) is significantly different from isotropic, but is dominated by photons of $\mu = 1$. This result is consistent with the “single shot picture” (Adams 1975; Bonilha et al. 1979), in which photons with frequency $|x| < 2$ mainly undergo a diffusion in the frequency space; once a photon diffuses to $|x| \geq 2$, it will take “single longest excursion” to leave for outside of the halo.

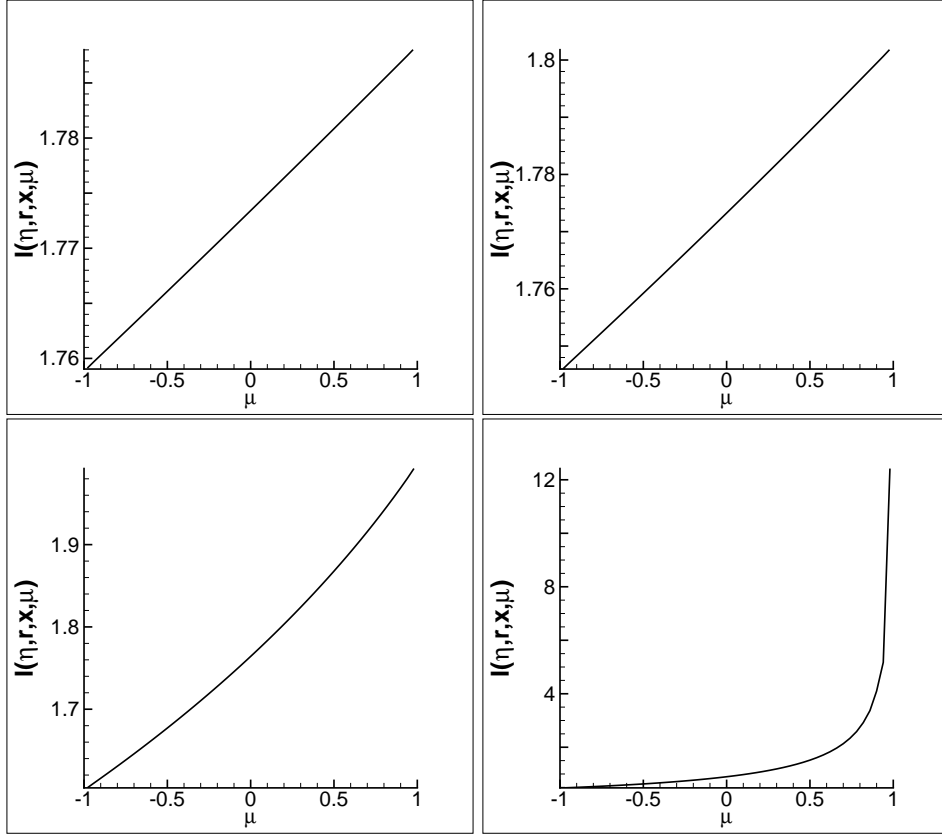


Fig. 5.— The μ distribution of photons emergent from a halo with radius $R = 500$. The frequencies are $x = 0.0$ (top left); 0.8 (top right); 1.6 (bottom left) and 2.4 (bottom right). The relevant parameters of the calculation are $\eta = 1.2 \times 10^4$, $\gamma = 0$, and $a = 10^{-3}$.

Therefore, the two peaks of the flux f at frequency $x_{\pm} \simeq \pm(2 - 3)$ are dominated by photons from “single longest excursion” photons, of which $\mu \sim 1$.

4.2. Dependence of the initial anisotropy

The source of Fig. 5 given by eq.(20) has $\Theta(\mu) = 6\mu$ ($\mu > 0$), which is linear of μ . We now consider sources with higher anisotropy with $\Theta(\mu)$ given by

$$\Theta(\mu) = \begin{cases} 2(n+2)\mu^n, & 0 < \mu \leq 1, \\ 0, & \mu < 0. \end{cases} \quad (22)$$

When the integer n is large, $\Theta(\mu)$ is similar to a δ function $\delta(\mu - 1)$, i.e. most photons are in the direction $\mu = 1$.

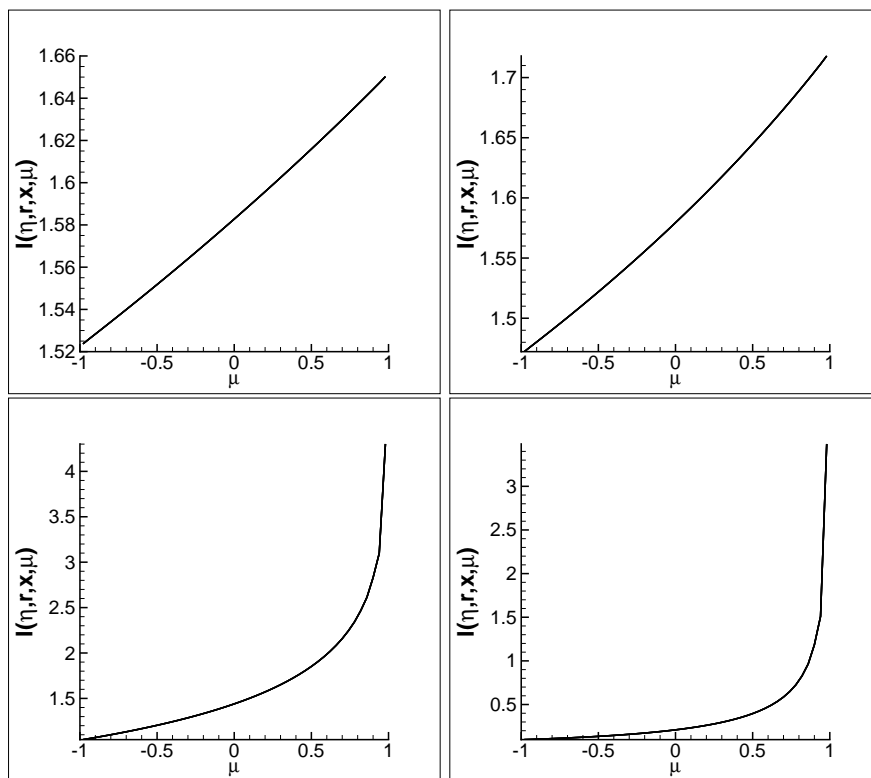


Fig. 6.— The μ -distribution of halo with radius $R = 100$ and source eq.(22) with $n=1, 2, 4,$ and 6 . The frequencies are taken to be $x = 0$ (top left), 0.8 (top right), 1.6 (bottom left), 2.4 (bottom right). The parameters of the halos are $\eta = 3500$, $\gamma = 0$, and $a = 10^{-3}$.

We repeat the calculation of Fig.5, but using the source eq.(22) with $n = 1, 2, 4$ and 6 . The result is plotted in Fig. 6. It is interesting to see that the μ -distributions are independent of n , but only depend on x . It is easy to explain the n -independence of the two top panels of Fig.6, both of which have frequency $|x| \leq 2$. In this frequency range, the evolution of the specific intensity I is governed by the local thermalization of x -space and entropy increasing of μ -space. These processes lead to the Boltzmann distribution in the energy space and isotropic distribution in the angular space, regardless of the initial distributions in either frequency- or angular spaces. In other words, the initial distribution is forgotten during the local thermalization and approaching statistical equilibrium.

However, the mechanism of the local thermalization and approaching isotropic distribution seems to be unable to explain why the two bottom panels of Fig. 6. also show n -independence. The μ -distribution of the two bottom panels of Fig. 6 are highly anisotropic. Therefore, they do not have to be the result of the local thermalization and approaching statistical equilibrium. Why do

they also show the behavior of forgetting the initial angular distributions? The reason is as follows. In the first phase of resonant photon evolution, Ly α photons are trapped in the range of $|x| \leq 2$ within the time scales of a few tens or hundred scattering (Roy et al. 2009c). The trapped photons have already forgotten their initial state. On the other hand, photons with $|x| \geq 2$ mostly come from the diffusion of trapped photons from $|x| \leq 2$ to $|x| \geq 2$ (Roy et al. 2009b). Thus, all photons of $|x| \geq 2$ emergent from the optically thick halo essentially have the same initial condition, given by the $|x|$ space diffusion of trapped photons. Therefore, the initial distributions before they are trapped have been forgotten. This property can also be seen in Fig. 2, in which, although the sources of the middle and right panels are different from each other, the behaviors of the time-evolution of the μ -distribution are about the same. This result also implies that it is impossible to find the information of the distribution of photons emitted by the central source.

4.3. Collimation of photons of the double peaks

A common feature of the two bottom panels of Fig. 6 is to show a very sharp spike at $\mu \sim 1$. The photon frequencies of the two panels are at $|x| = 1.6$ and $|x| = 2.4$, corresponding to the double peaks of Figs 3 and 4. Therefore, the spiky distribution of μ indicates that the photons with frequency at the double peaks have formed a forward beam.

In order to measure the angular size of the $\mu = 1$ spikes, we fit the μ -distributions of the two bottom panels of Fig. 6 with polynomials of μ . We find that both the two bottom panels of Fig. 6 can be well fitted with polynomials of μ having leading terms $A\mu^{16} + B\mu^{15} + \dots$, A, B being fitting coefficients. The terms of either μ^{16} or μ^{15} are much sharper than the central source eq.(22) μ^n with $n \leq 6$. Therefore, the radiative transfer at the double peaks of frequency space plays the role of forward collimator. It made the photons to form forward beams.

If we define the spread angle β of the forward beam as the angle of half intensity, this number can be estimated by $\sin\beta \sim (1/2)^{16}$, and therefore, $\beta \sim 10^{-4}$ angular degree. This result is again consistent with the “single shot picture”. The double peaks mainly consist of photons from a single shot, which moves in the forward direction.

4.4. Large halo

We calculate the μ -distribution of Ly α photons in a halo with large radius $R = 1000$, and the central source is given by eq.(22) and $n = 6$. The results are given in Fig. 7, which shows the dependence of the μ distribution on the radial variable r in the halo.

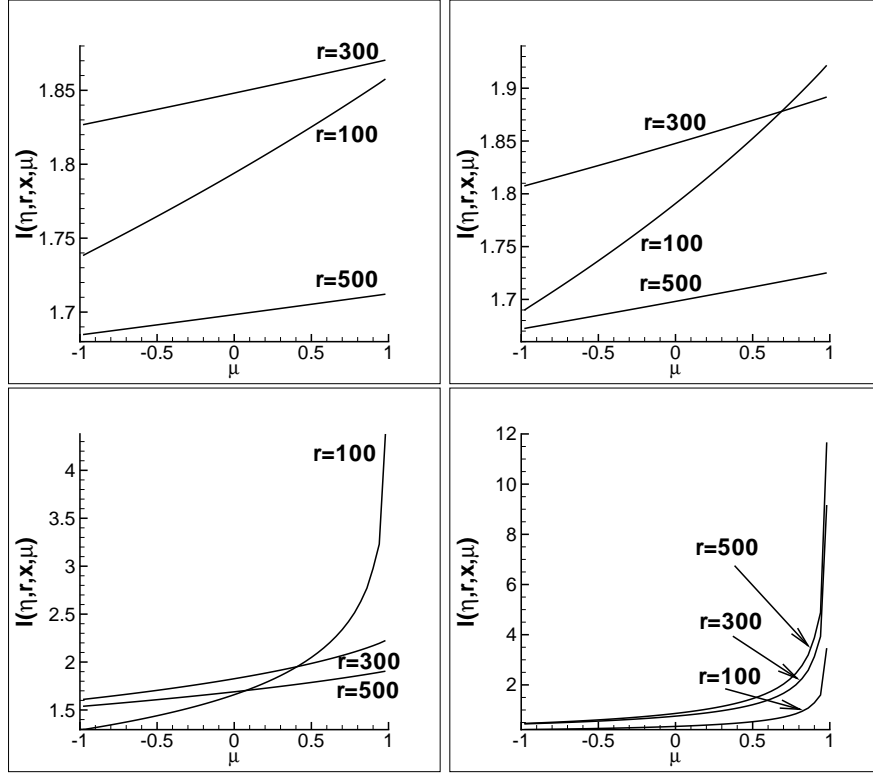


Fig. 7.— The μ -distributions at radial positions $r = 100, 300, 500$ of a halo with radius $R = 1000$. The source is given by eq.(22) and $n = 6$. The frequencies are taken to be $x = 0$ (top left), 0.8 (top right), 1.6 (bottom left), 2.4 (bottom right). Other relevant parameters are $\eta = 1.2 \times 10^4$, $\gamma = 0$ and $a = 10^{-3}$.

Although the photons from the source of $n = 6$ are highly anisotropic, all the μ -distributions of $x = 0.0$ and 0.8 at $r = 100, 300, 500$ are straight lines. That is, the specific intensity I can be well approximated by the Eddington approximation eq.(10). This result is consistent with §4.2. The slope of the straight line is decreasing with the radial position. It is simply because for a stable solution, the photon number is conserved, and the flux should be smaller at larger r . The r -dependence of the μ -distribution of $|x| = 2.4$ photons is also consistent with the result of section 4.3: the larger the r , the sharper the μ -distribution. The r transfer leads to the collimation.

The behavior of r -dependence of the μ -distribution at $x = 1.6$ (bottom left of Fig. 7) is very different from that of $x = 0.0, 0.8$, and 2.4 . The μ distribution at $r = 100$ is about the same as the bottom right panel of Fig. 6, i.e. it has undergone an evolution of forward collimation, having a sharp spike at $\mu = 1$. However, the μ distribution will no longer show a spike at $r = 300$ and 500 . That is, the r -dependence of the bottom left panel shows two phases. When r is equal to or less

than about 200, the r -dependence of the μ distribution is similar to the $|x| = 2.4$ photons. While when $r \geq 200$, the r -dependence of μ distribution is similar to the $|x| = 0$ and 0.8 photons. This is because the optical depth at $|x| = 1.6$ is larger than $|x| = 2.4$, the “single shot picture” is working well at $r \sim 100$ for both $|x| = 1.6$ and 2.4. However, at $r \geq 200$, the single shot picture can still work well for $|x| = 2.4$, but not so well for $|x| = 1.6$.

4.5. Effect of anisotropic scattering

All calculations in the previous sections are based on the re-distribution function eq.(4), which considered only isotropic scattering. If we consider dipole scattering, it seems to introduce a new factor leading to anisotropic. However, the re-distribution function of dipole scattering eq.(5) actually is independent of μ . It does not change any of the results mentioned above. The dipole scattering of individual atoms may yield new anisotropic behavior. However, HI atoms are in thermal equilibrium, and their distribution is isotropic. The dipole scattering, in average, does not contain any parameter of specific direction. It will not add any anisotropic behavior. Therefore, all conclusions in the previous sections should still hold.

5. Conclusion

The transfer of Ly α resonant photons from a central source in a halo consisting of HI generally is considered as a problem of radiative transfer in an optically thick medium. However, the “optically thick medium” is true only when the frequency of Ly α photons lies in a narrow range $|x| \leq 2$. The cross section of resonant scattering is very sensitive to the photon frequency. It quickly becomes small when the frequency of Ly α photons has only a small deviation from the range $|x| \leq 2$. For those photons, the halo is optically moderate thick, or even thin. Therefore, in order to understand the transfer of Ly α photons with frequency around the resonant peak, we need to find the solutions of the integro-differential equation (1) available simultaneously in optically thick as well as moderate thick and even thin medium. That is, although halo is optically thick for resonant photons, one should not treat eq.(1) by using the condition of optical thick.

To find solution of eq.(1) having desired precision in frequency ranges of optically thick as well as moderately thick, the algorithm should be able to handle the extremely flat distribution ($|x| < 2$) and its sharp boundary ($|x| \sim 2$) of I . These features can be properly captured by the state-of-the-art numerical method, WENO scheme, as it has high order of accuracy and good convergence in capturing discontinuities as well as to be significantly superior over piecewise smooth solutions containing discontinuities. The WENO solver has been shown to be powerful to solve

the integro-differential equation of radiative transfer of resonant photons $\text{Ly}\alpha$. In this paper, we develop the WENO algorithm to be able to solve the integral-differential equation (1) in frequency and angular space simultaneously.

We first show that the Eddington approximation can yield reasonable results of the frequency profile of photons emergent from optically thick halos. Since the Eddington approximation is to assume that I linearly depends on μ , all the physics of the angular distribution of $\text{Ly}\alpha$ photons are missing. A cost of the Fokker-Planck equations is also to ignore all the effects of the evolutions of angular distribution.

The physics of the evolution of angular distribution is rich. As has been known, resonant scattering makes the transfers of resonant photons in the physical space and the frequency space to be coupled between each other. We show, in this paper, that the resonant scattering leads to the coupling between the evolutions of resonant photons in the frequency space and the angular space as well. The evolution of resonant photon distribution in the μ space is significantly dependent on the frequency. Photons with frequency $|x| \leq 2$ undergo the procedure of approaching statistical equilibrium, and their angular distribution is isotropic after a few tens or hundred scattering, regardless of whether the initial angular distribution is isotropic. On the other hand, the angular distribution of photons with $|x| \geq 2$ is substantially anisotropic, even if the initial angular distribution is isotropic.

An interesting feature is that the anisotropic angular distributions at frequency $|x| \sim 2$ are independent of the initial angular distributions. Different initial angular distributions yield the same anisotropic angular distributions after a few tens or hundred scattering. This is because photons at frequency $|x| \sim 2$ are not directly from the source, but come from the trapped photons within $|x| \leq 2$, for which the initial distributions have been forgotten. Therefore, it seems to be impossible to find the property of the source with the observed μ -distribution of $\text{Ly}\alpha$ photons either in the range of $|x| \leq 2$ or in $|x| \geq 2$.

Another interesting feature of an optically thick halo is the collimation of photons with frequency of the double peaks. This is also because photons trapped in $|x| \leq 2$ are thermal. When the trapped photons diffuse to $|x| \geq 2$, they have two possible fates. One is to get out of the holes by a single shot if photons move forward. If a photon has not taken a single shot, the resonant scattering will lead it to get back to the region of $|x| \leq 2$. Therefore, photon transfer in optically thick medium is a collimator. Although photons stored in an optically thick halo are thermal, the μ -distribution is isotropic, the double peak is only to pick up photons of single shot, i.e. moving forward.

Acknowledgment: This research is partially supported by ARO grants W911NF-08-1-0520 and W911NF-11-1-0091.

A. Numerical algorithm

To solve equation (1), our computational domain is $(r, x, \mu) \in [0, r_{\max}] \times [x_{\text{left}}, x_{\text{right}}] \times [-1, 1]$, where r_{\max} , x_{left} and x_{right} are chosen such that the solution vanishes to zero outside the boundaries. We choose mesh sizes with grid refinement tests to ensure proper numerical resolution. In the following, we describe numerical techniques involved in our algorithm, including approximations to spatial derivatives, numerical integration, numerical boundary condition and time evolution.

A.1. Conservation law

To perform the WENO algorithm, we first need to rewrite the equation into the form of a conservation law. Noticing the boundary condition (14), we define $I' = r^2 I$, then equation (1) becomes

$$\begin{aligned} \frac{\partial I'}{\partial \eta} + \mu \frac{\partial I'}{\partial r} + \frac{1}{r} \frac{\partial(1 - \mu^2)I'}{\partial \mu} - \gamma \frac{\partial I'}{\partial x} = \\ -\phi(x; a)I' + \int \mathcal{R}(x, x'; a)I'(\eta, r, x', \mu')dx'd\mu'/2 + r^2 S. \end{aligned} \quad (\text{A1})$$

For simplicity, we drop the prime, and use $I(\eta, r, x, \mu)$ for $I'(\eta, r, x, \mu)$ below.

A.2. The WENO algorithm: approximations to the spatial derivatives

The spatial derivative terms in equation (A1) are approximated by a fifth-order finite difference WENO scheme.

We first give the WENO reconstruction procedure in approximating $\frac{\partial I}{\partial x}$,

$$\frac{\partial I(\eta^n, r_i, x_j, \mu_k)}{\partial x} \approx \frac{1}{\Delta x} (\hat{h}_{j+1/2} - \hat{h}_{j-1/2})$$

with fixed $\eta = \eta^n$, $r = r_i$ and $\mu = \mu_k$. The numerical flux $\hat{h}_{j+1/2}$ is obtained by the fifth-order WENO approximation in an upwind fashion, because the wind direction is fixed (negative). Denote

$$h_j = I(\eta^n, r_i, x_j, \mu_k), \quad j = -2, -1, \dots, N_x + 3$$

with fixed n , i and k . The numerical flux from the WENO procedure is obtained by

$$\hat{h}_{j+1/2} = \omega_1 \hat{h}_{j+1/2}^{(1)} + \omega_2 \hat{h}_{j+1/2}^{(2)} + \omega_3 \hat{h}_{j+1/2}^{(3)}, \quad (\text{A2})$$

where $\hat{h}_{j+1/2}^{(m)}$ are the three third-order fluxes on three different stencils given by

$$\begin{aligned}\hat{h}_{j+1/2}^{(1)} &= -\frac{1}{6}h_{j-1} + \frac{5}{6}h_j + \frac{1}{3}h_{j+1}, \\ \hat{h}_{j+1/2}^{(2)} &= \frac{1}{3}h_j + \frac{5}{6}h_{j+1} - \frac{1}{6}h_{j+2}, \\ \hat{h}_{j+1/2}^{(3)} &= \frac{11}{6}h_{j+1} - \frac{7}{6}h_{j+2} + \frac{1}{3}h_{j+3},\end{aligned}$$

and the nonlinear weights ω_m are given by

$$\omega_m = \frac{\check{\omega}_m}{\sum_{l=1}^3 \check{\omega}_l}, \quad \check{\omega}_l = \frac{\gamma_l}{(\epsilon + \beta_l)^2},$$

where ϵ is a parameter to avoid the denominator to become zero and is taken as $\epsilon = 10^{-8}$. The linear weights γ_l are given by

$$\gamma_1 = \frac{3}{10}, \quad \gamma_2 = \frac{3}{5}, \quad \gamma_3 = \frac{1}{10},$$

and the smoothness indicators β_l are given by

$$\begin{aligned}\beta_1 &= \frac{13}{12}(h_{j-1} - 2h_j + h_{j+1})^2 + \frac{1}{4}(h_{j-1} - 4h_j + 3h_{j+1})^2, \\ \beta_2 &= \frac{13}{12}(h_j - 2h_{j+1} + h_{j+2})^2 + \frac{1}{4}(h_j - h_{j+2})^2, \\ \beta_3 &= \frac{13}{12}(h_{j+1} - 2h_{j+2} + h_{j+3})^2 + \frac{1}{4}(3h_{j+1} - 4h_{j+2} + h_{j+3})^2.\end{aligned}$$

Similarly, we give the WENO procedure in approximating $\frac{\partial(1-\mu^2)I}{\partial\mu}$,

$$\frac{\partial(1-\mu_j^2)I(\eta^n, r_i, x_k, \mu_j)}{\partial\mu} \approx \frac{1}{\Delta\mu}(\hat{h}_{j+1/2} - \hat{h}_{j-1/2})$$

with fixed $\eta = \eta^n$, $r = r_i$ and $x = x_k$. The numerical flux $\hat{h}_{j+1/2}$ is also obtained by the fifth-order WENO approximation in an upwind fashion, however the wind direction here is positive, opposite from that of $\frac{\partial I}{\partial x}$. Denote

$$h_j = (1 - \mu_j^2)I(\eta^n, r_i, x_k, \mu_j), \quad j = -3, -2, \dots, N_\mu + 2$$

with fixed n , i and k . The numerical flux from the WENO procedure is obtained by

$$\hat{h}_{j+1/2} = \omega_1 \hat{h}_{j+1/2}^{(1)} + \omega_2 \hat{h}_{j+1/2}^{(2)} + \omega_3 \hat{h}_{j+1/2}^{(3)}, \quad (\text{A3})$$

where $\hat{h}_{j+1/2}^{(m)}$ are the three third-order fluxes on three different stencils given by

$$\begin{aligned}\hat{h}_{j+1/2}^{(1)} &= -\frac{1}{6}h_{j+2} + \frac{5}{6}h_{j+1} + \frac{1}{3}h_j, \\ \hat{h}_{j+1/2}^{(2)} &= \frac{1}{3}h_{j+1} + \frac{5}{6}h_j - \frac{1}{6}h_{j-1}, \\ \hat{h}_{j+1/2}^{(3)} &= \frac{11}{6}h_j - \frac{7}{6}h_{j-1} + \frac{1}{3}h_{j-2},\end{aligned}$$

and the nonlinear weights ω_m are given by

$$\omega_m = \frac{\check{\omega}_m}{\sum_{l=1}^3 \check{\omega}_l}, \quad \check{\omega}_l = \frac{\gamma_l}{(\epsilon + \beta_l)^2},$$

where ϵ is taken as $\epsilon = 10^{-8}$. The linear weights γ_l are also given by

$$\gamma_1 = \frac{3}{10}, \quad \gamma_2 = \frac{3}{5}, \quad \gamma_3 = \frac{1}{10},$$

and the smoothness indicators β_l are given by

$$\begin{aligned}\beta_1 &= \frac{13}{12}(h_{j+2} - 2h_{j+1} + h_j)^2 + \frac{1}{4}(h_{j+2} - 4h_{j+1} + 3h_j)^2, \\ \beta_2 &= \frac{13}{12}(h_{j+1} - 2h_j + h_{j-1})^2 + \frac{1}{4}(h_{j+1} - h_{j-1})^2, \\ \beta_3 &= \frac{13}{12}(h_j - 2h_{j-1} + h_{j-2})^2 + \frac{1}{4}(3h_j - 4h_{j-1} + h_{j-2})^2.\end{aligned}$$

In the end, we approximate the r -derivative in equation (A1), following the reconstruction procedures mentioned above. However, we need to check the wind direction at the r -boundary of each cell. When $\mu > 0$, the wind direction is positive, then we use equation (A3) to approximate the numerical flux, while when $\mu < 0$, we use equation (A2).

A.3. High order numerical integration

The integration of the resonance scattering term is calculated by a fifth order quadrature (Shen et al.2007)

$$\int_{\mu_{left}}^{\mu_{right}} f(\mu)d\mu = \Delta\mu \sum_{k=1}^{N_\mu} \omega_k f(\mu_k) + O(\Delta\mu^5),$$

where $\mu_k = \mu_{left} + (k - \frac{1}{2})d\mu$ and the weights are defined as,

$$\begin{aligned} \omega_1 &= \frac{6463}{5760}, & \omega_2 &= \frac{1457}{1920}, & \omega_3 &= \frac{741}{640}, & \omega_4 &= \frac{5537}{5760}, \\ \omega_{N_\mu-3} &= \frac{5537}{5760}, & \omega_{N_\mu-2} &= \frac{741}{640}, & \omega_{N_\mu-1} &= \frac{1457}{1920}, & \omega_{N_\mu} &= \frac{6463}{5760}, \end{aligned}$$

and $\omega_k = 1$ otherwise.

A.4. Numerical boundary condition

Following Carrillo et al. (2006), at $\mu = -1$ and $\mu = 1$, we take the boundary conditions as, for $\mu > 0$,

$$\begin{aligned} I(\eta, r, x, -1 - \mu) &= I(\eta, r, x, -1 + \mu), \\ I(\eta, r, x, 1 + \mu) &= I(\eta, r, x, 1 - \mu), \end{aligned}$$

motivated by the physical meaning of μ as the cosine of the angle to the z -axis. We also explicitly impose $\hat{h}_{\frac{1}{2}} = \hat{h}_{N_\mu+\frac{1}{2}} = 0$ for the first and last numerical fluxes in order to enforce conservation of mass.

A.5. Time evolution

To evolve in time, we use the third-order TVD Runge-Kutta time discretization (Shu & Osher 1988). For system of ODEs $u_t = L(u)$, the third order Runge-Kutta method is

$$\begin{aligned} u^{(1)} &= u^n + \Delta\tau L(u^n, \tau^n), \\ u^{(2)} &= \frac{3}{4}u^n + \frac{1}{4}(u^{(1)} + \Delta\tau L(u^{(1)}, \tau^n + \Delta\tau)), \\ u^{n+1} &= \frac{1}{3}u^n + \frac{2}{3}(u^{(2)} + \Delta\tau L(u^{(2)}, \tau^n + \frac{1}{2}\Delta\tau)). \end{aligned}$$

REFERENCES

- Adams, T.F. 1975, ApJ, 201, 350
 Adams, T.F., Hummer, D.G. & Rybicki, G.B. 1971, J. Quant. Spectrosc. Radiat. TransferApJ, 11, 1365

- Bonilha, J. R. M., Ferch, R., Salpeter, E. E., Slater, G., Noerdlinger, P. D. 1979, ApJ233, 649
- Carrillo, J. Gamba, I., Majorana, A., Shu, C.-W., 2006, J. Comp. Phys. 214, 55
- Dijkstra, M., Haiman, Z. & Spaans, M. 2006, ApJ, 649, 14
- Dijkstra, M. & Loeb, A. 2009, MNRAS, 400, 1109
- Fang, L.Z., 2009, Inter. J. Mod. Phys. D18, 1943
- Fardal et al. 2001, ApJ, 562, 505
- Field, G.B., 1958, Proc. IRE, 46, 240
- Field, G.B. 1959, ApJ, 129, 551.
- Haiman, Z. et al. 2000, ApJ, 537, 5
- Harrington, J.P. 1973, MNRAS, 162, 43
- Heney, L. G. & Greestein, J. L. 1941, AJ, 93, 70
- Hummer, D.G. 1962, MNRAS, 125, 21
- Hummer, D.G. 1965, Mem. R. astr. Soc., 70, 1
- Hummer, D.G. 1969, MNRAS, 145, 95
- Jiang, G. & Shu, C.-W. 1996, J. Comput. Phys., 126, 202
- Latif, M. et al. 2011, MNRAS, 413, L33
- Laursen, P., & Sommer-Larsen J. 2007, ApJ, 657, L69
- Loeb, A. & Rybicki, G. 1999, ApJ, 524, 527
- Neufeld, D. A. 1990, ApJ, 350, 216
- Osterbrock, D.E. 1962, ApJ, 135, 195
- Pierleoni, M., Maselli, A., & Ciardi B. 2009, MNRAS, 393, 872
- Roy, I., Qiu J.-M., Shu C.-W. & Fang L.-Z., 2009a, New Astronomy 14, 513
- Roy, I. Xu, W., Qiu J.-M., Shu C.-W. & Fang L.-Z., 2009b, ApJ, 694, 1121
- Roy, I. Xu, W., Qiu J.-M., Shu C.-W. & Fang L.-Z., 2009c, ApJ, 703, 1992
- Roy, I, Shu, C.-W. & Fang, L. Z. 2010, ApJ, 716, 604
- Rybicki, G.B. & Dell'Antonio, I.P. 1994, ApJ, 427, 603
- Rybicki G.B. & Lightman, 1979, Radiative Processes in Astrophysics, (J. Wiley New York).
- Shen J., Shu C.-W., Zhang M., 2007, J. Sci. Comput., 33,279
- Shu, C.-W. & Osher, S., 1988, J. Comput. Phys., 77, 439

- Spitzer, L. & Greenstein, J.L. 1951, *ApJ*, 114, 407
- Tasitsiomi, A. 2006, *ApJ*, 645, 792
- Unno, W. 1955, *Publ. Astron. Soc. Japan*. 7, 81
- Verhamme, A., Schaerer, D. & Maselli, A. 2006, *AA*, 460, 397
- Wouthuysen, S. A. 1952, *AJ*, 57, 31
- Xu, W. & Wu, X.-P. 2010, *ApJ*, 710, 1432
- Xu, W, Wu, X.-P. & Fang, L.Z., 2011, *MNRAS*, 418, 853
- Yang, Y., Roy, I., Shu, C.-W. & Fang, L.Z. 2011, *ApJ*, 739, 91
- Zheng, Z. & Miralda-Escude, J., 2002, *ApJ*, 578, 33